Endogenous modulation of low frequency oscillations by temporal expectations

Andre M. Cravo, Gustavo Rohenkohl, Valentin Wyart and Anna C. Nobre

J Neurophysiol 106:2964-2972, 2011. First published 7 September 2011; doi:10.1152/jn.00157.2011

J Neurophysiol 106: 2964–2972, 2011.
First published September 7, 2011; doi:10.1152/jn.00157.2011.

Endogenous modulation of low frequency oscillations by temporal expectations

Andre M. Cravo,[1] Gustavo Rohenkohl,[2,3] Valentin Wyart,[2] and Anna C. Nobre[2,3]
[1]*Department of Physiology and Biophysics, University of São Paulo, São Paulo, Brazil; and* [2]*Department of Experimental Psychology and* [3]*Oxford Centre for Human Brain Activity, University of Oxford, Oxford, United Kingdom*

Submitted 23 February 2011; accepted in final form 6 September 2011

Cravo AM, Rohenkohl G, Wyart V, Nobre AC. Endogenous modulation of low frequency oscillations by temporal expectations. *J Neurophysiol* 106: 2964–2972, 2011. First published September 7, 2011; doi:10.1152/jn.00157.2011.— Recent studies have associated increasing temporal expectations with synchronization of higher frequency oscillations and suppression of lower frequencies. In this experiment, we explore a proposal that low-frequency oscillations provide a mechanism for regulating temporal expectations. We used a speeded Go/No-go task and manipulated temporal expectations by changing the probability of target presentation after certain intervals. Across two conditions, the temporal conditional probability of target events differed substantially at the first of three possible intervals. We found that reactions times differed significantly at this first interval across conditions, decreasing with higher temporal expectations. Interestingly, the power of theta activity (4–8 Hz), distributed over central midline sites, also differed significantly across conditions at this first interval. Furthermore, we found a transient coupling between theta phase and beta power after the first interval in the condition with high temporal expectation for targets at this time point. Our results suggest that the adjustments in theta power and the phase-power coupling between theta and beta contribute to a central mechanism for controlling neural excitability according to temporal expectations.

temporal expectations; phase-power coupling; neural oscillations

THE ABILITY TO PROGRAM AND update actions according to the expected timing of forthcoming events is essential for behavior. In the motor domain, it is increasingly recognized that expectations change according to type of movement and its expected timing (Cotti et al. 2011; Cui et al. 2009; Nobre et al. 2007; Praamstra et al. 2006; Riehle et al. 1997). The state of motor preparation and its dynamic modulation are reflected in the oscillatory rhythm in the beta range (15–30 Hz) on the motor cortex (Pfurtscheller et al. 1996; Sanes and Donoghue 1993; Swann et al. 2009; Tzagarakis et al. 2010; Wang 2010). Accordingly, studies investigating the oscillatory correlates of motor preparation and temporal expectations have focused on frequencies in this range (Alegre et al. 2006; Praamstra et al. 2006; van Ede et al. 2011).

However, recent studies have proposed that rhythmic or regular stimulus events are able to entrain low-frequency rhythms (e.g., in the delta and theta ranges), which in turn regulate the excitability of higher frequency rhythms (e.g., in the beta and gamma ranges) so that cortical excitability is optimized for processing relevant upcoming events (Lakatos et al. 2005, 2007, 2008; Schroeder and Lakatos 2009). Additionally, it has been proposed that low-frequency cortical oscillations may contribute to slow event-related potentials (ERPs), such as the contingent negative variation (CNV; Praamstra et al. 2006; Schroeder and Lakatos 2009). The CNV is a potential generated in motor-related areas that occurs in anticipation of stimuli or responses (Los and Heslenfeld 2005; Miniussi et al. 1999; Pfeuty et al. 2005; Trillenberg et al. 2000; Walter et al. 1964). Neurophysiological studies have associated the CNV with "hazard rates," the conditional probability of an event occurring at a specific time given that it has not yet occurred (Janssen and Shadlen 2005; Luce 1986; Nobre et al. 2007).

We investigated whether low-frequency oscillations and the CNV potential varied systematically according to the temporal hazard rates inherent in the structure of a simple motor task. Additionally, we tested whether motor excitability, reflected in the beta-band activity, was modulated by these low-frequency oscillations. We used a Go/No-go reaction-time task where participants had to respond or withhold responses to targets presented after a warning signal (WS). The distribution of foreperiod (FP) intervals between WS and targets was manipulated across two experimental conditions, so that target events were much more likely to occur at the first of three possible intervals in one condition (*U*-shaped distribution) than another (negatively skewed distribution). We compared the temporal development of the CNV, of the power of low-frequency oscillations, and of the nesting of beta within these low-frequency carrier oscillations. Our findings suggest that low-frequency oscillations play a key role in temporal expectations, reflected by an increase in power and by a phase reset of theta oscillations. Furthermore, we found a coupling of low-frequency oscillations with the power of beta oscillations in task-relevant instants, indicating a functional role of this nesting as a mechanism for motor updating.

MATERIALS AND METHODS

Participants. Twelve participants (aged 23–34, 8 females, all right-handed) gave informed consent to take part in the experiment. Visual acuity was normal or corrected-to-normal. All experimental methods had ethical approval from the Central University Research Ethics Committee of the University of Oxford.

Stimuli and task. Participants sat in a dimly illuminated and electrically shielded room, positioned at a 100-cm distance from the screen. The stimuli were presented using Presentation software (version 12.2, www.neurobs.com) on a 21-in cathode ray tube monitor (CTX ultra screen). The experimental session lasted ~1 h. Participants were instructed to maintain central fixation throughout the whole experiment. Eye movements were monitored online with a remote video-based infrared eye-tracker and electrooculogram (EOG). Trials with eye movements were very rare (<1% of trials) and were discarded from the analysis.

Participants performed a simple Go/No-go task. Across two blocked conditions, we manipulated temporal expectations for the appearance of the imperative stimulus by varying the temporal conditional probability of the target event across three intervals. The

Address for reprint requests and other correspondence: A. C. Nobre, Brain and Cognition Lab., Dept. of Experimental Psychology, South Parks Rd., Oxford OX1 3UD, UK (e-mail: kia.nobre@psy.ox.ac.uk).

Go/No-Go paradigm encouraged participants to anticipate the target while still demanding that they wait for its presentation to respond.

Each experimental block started with a fixation cross in the center of the screen, which was replaced by a WS after a random interval between 500 and 1,000 ms (Fig. 1*A*). After a FP of 1.25, 2.25, or 3.25 s, the WS became filled with blue (Go target) on 80% of the trials or with red (No-Go Target) on 20% of the trials. Participants pressed a button with their right index finger as quickly as possible when a Go target appeared (80% of trials) and refrained from responding to No-go targets (remaining 20% of trials). After 200 ms, the target was replaced by the fixation cross, which remained on the screen for a random interval between 1,000 and 2500 ms, when a new WS was presented.

The FPs were randomized from trial to trial, according to a probability distribution that remained constant throughout the block. Two probability distributions were used. In the negatively skewed distribution, the target had a 0.10, 0.45, and 0.45 probability of being presented at 1.25, 2.25, or 3.25 s after the WS, respectively. In the *U*-shaped distribution, the probabilities were 0.45, 0.10, and 0.45, respectively (Fig. 1*B*). Each probability distribution had a particular WS, which was either an empty square or an empty diamond (1°). For half of the participants, the square was used for the negatively skewed distribution, while for the other half it was used for the *U*-shaped distribution.

The anticipation for each target can be expressed in terms of the hazard rate. This is calculated as the probability that the target will occur at time *t* divided by the probability that it has not yet occurred (Luce 1986). Based on the assumption that elapsed time is known with uncertainty that scales with the magnitude of the temporal interval (Gibbon 1977; Killeen and Weiss 1987), we calculated "subjective" hazard rates, also referred as anticipation functions (Janssen and Shadlen 2005). Figure 1*B* shows how the anticipation functions associated with the two probability distributions were clearly different. In both functions, anticipation increases as a function of the FP. Importantly, anticipation functions differ markedly for the first FP between the two probability distributions, where there is a higher anticipation in the *U*-shaped compared with the negatively skewed distribution. The anticipation functions are much more similar at the later FPs.

Participants were tested on the different probability distributions (negatively skewed and *U*-shaped) on the same day, with the blocks of each distribution being presented sequentially. The order of the probability distributions was counterbalanced between participants. The experimental session consisted of 10 blocks of 60 trials each (1 practice block and 4 experimental blocks for each probability distribution).

EEG recording. The EEG was acquired continuously from 35 Ag/AgCl electrodes at 1,000 Hz referenced to the right mastoid site (AFZ ground; 300-Hz low-pass filter). The electrodes were positioned according to the 10–05 International system (AEEGS 1991) and recorded using NuAmp amplifiers (Neuroscan, El Paso, TX). Electrode impedances were kept <5 kΩ. The montage included seven midline sites (Fz, FCz, Cz, CPz, Pz, POz, and OZ) and 14 sites over each hemisphere (FP1/FP2, F1/F2, F3/F4, FC1/FC2, FC3/FC4, C1/C2, C3/C4, CP1/CP2, CP3/CP4, P1/P2, P3/P4, PO3/PO4, PO7/PO8, and O1/O2). Six additional electrodes were used as ground and reference sites and for recording the EOG. EOG electrodes were placed to the side of each eye [horizontal EOG (HEOG)] and above and below the left eye [vertical EOG (VEOG)], and bipolar signals were subsequently derived by computing the difference between these electrodes. Eye movements and blinks were also monitored using a remote, video-based infrared eye tracker (ISCAN, ETL-400 system, 60 Hz).

EEG processing and analysis. All ERP processing were performed using Neuroscan version 4.3. To perform the CNV analysis, continuous EEG was re-referenced to the algebraic average of the right and left mastoids and filtered offline with a 40-Hz low-pass filter (24 db/oct). The analysis was performed on trials in which it was possible to examine the evolution of this potential across FPs and for the maximal amount of time. Only trials in which the target (Go or No-Go) appeared after the longest FP (3.25 s) were included. In this way, we were able to examine how the different anticipation functions

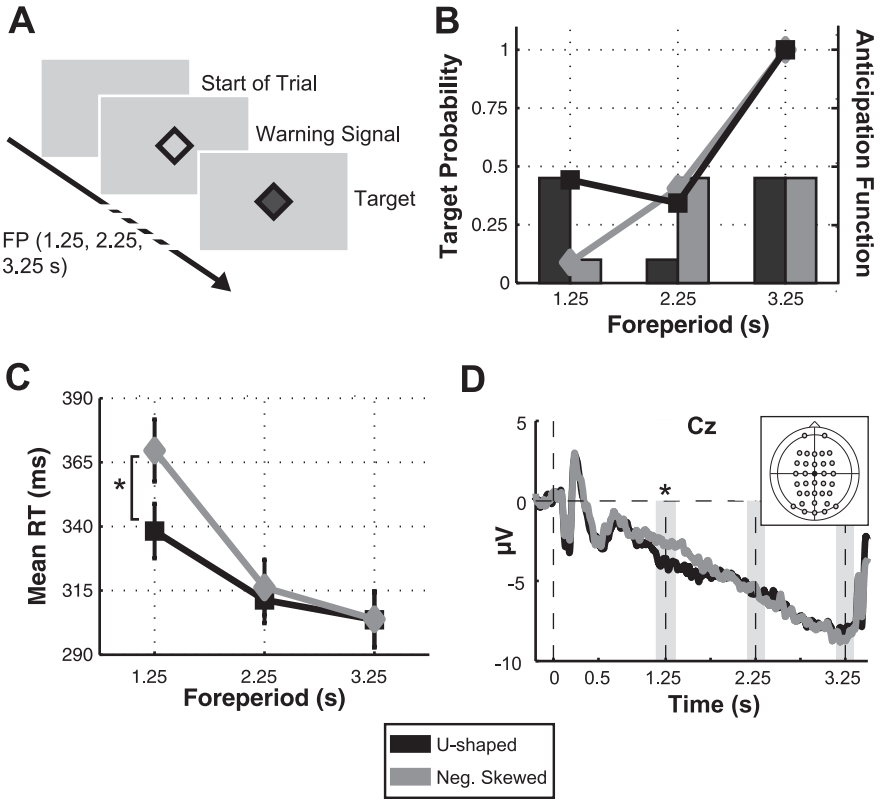

Fig. 1. Experimental paradigm. *A*: participants viewed a warning signal (WS) followed by a Go/No-go target at either 1.25, 2.25, or 3.25 s after the WS onset. *B*: target probability and anticipation functions for both experimental conditions. Bar plots represent the physical probability of target presentation after the 3 possible foreperiods (FPs). Line plots represent the anticipation functions (Janssen and Shadlen 2005) for each probability distribution. *C*: reaction times (means ± SE) for each FP and probability distribution. There was a significant difference between distributions only in the first FP. *D*: grand-averaged waveforms elicited by targets presented after the longest FP (3.25 s). Results showed significant difference between the contingent negative variation between probability distributions in the period around the first FP. RT, reaction time.

modulated this potential without the signal being contaminated by potentials related to cue or target processing.

ERPs elicited from the long FP trials were first epoched from −500 to 5,000 ms relative to the onset of the warning cue and linear detrended to correct each epoch for slow DC shifts (Poli et al. 2007). The epochs were then cut from −200 to 3,750 ms, relative to the warning cue onset. The precue interval from −200 ms to 0 ms was used to calculate the baseline for the ERP. Epochs containing excessive noise or drift (±100 μV at any electrode) or eye artefacts (blinks or saccades) were rejected. Blinks and saccades were identified as large deflections (±50 μV) in the horizontal or vertical EOG electrodes and subsequently checked by visual inspection. An average of 90 (minimum of 84) trials was obtained per subject for the negatively skewed and *U*-shaped distribution conditions.

The time-frequency analysis was performed on unfiltered data from the longest FP, epoched from −500 to 3,750 ms relative to the warning cue onset. Similarly to the ERP analysis, only trials where the target appeared after the longest FP (3.25 s) were analyzed. Phase and power estimates were computed by means of a continuous wavelet transform (length of 6 cycles) of single-trial data for the frequency range between 1 and 40 Hz (steps of 0.5 Hz). The power estimates were then averaged across trials for each condition and participant. The data from −250 ms to 0 relative to the onset of the WS were used as baseline. At each time sample and frequency, the log-transformed increase of signal power relative to baseline was considered as the measure of interest for the statistical analysis.

The phase-locking values (PLV) were estimated by averaging the normalized complex numbers across trials for each time point and frequency bin. These values describe the consistency of the phase angles with respect to the onset of an event.

Phase-power coupling. The analysis of phase-power coupling was completed in two steps. Firstly, phase values for theta (4 to 8 Hz) from electrode Cz were concatenated with power values of higher frequencies (10 to 30 Hz) at electrode C3, placed over motor cortex contralateral to the response hand. Phase and power values were collapsed for the period between 1 and 3 s after WS and between conditions. For each frequency of theta (from 4 to 8 Hz, in steps of 0.5 Hz), power values were sorted according to the phase angle of theta. Next, the phases were separated into 30 bins and the mean power over each frequency and bin was calculated. The mean powers within each frequency and participant were then z-transformed. Therefore, at this point we had the distribution of the power of each frequency over the 30 bins of the theta phase. We were interested in the correlation between phase angle of theta and the power of higher frequencies. Because phase values follow a circular distribution, we used a circular linear correlation measure (Berens 2009). Therefore, the *r*-square coefficient measures the correlation between theta phase angles and the z-transformed power of each frequency within that time window. The data from all subjects were pooled before calculating the circular-linear correlation. The *r*-squares were computed across subjects to extract only consistent phase-power couplings at the same phase value across subjects. If the phase-power coupling was not locked at the same phase value across subjects, the *r*-square would have been small, even if each subject had a strong phase-power coupling.

In a second step, we investigated the temporal dynamics of phase-power coupling in the different experimental conditions. The power values between 14 and 30 Hz from electrode C3 were concatenated with the instantaneous phase angle (from $-\pi$ to $+\pi$) from the theta oscillation where the coupling peaked (5 Hz) of electrode Cz. The same procedure as described in the first step was repeated for sequential time windows of 600 ms. This procedure was repeated for 200 partially overlapping windows, with their centers placed between 1 and 3 s, in 10-ms steps.

To assess the statistical difference of the *r*-squares between the experimental conditions, we performed a nonparametric cluster analysis (Maris and Oostenveld 2007). This analysis consists of clustering adjacent time-frequency samples that exhibit a similar difference (in sign and magnitude) between conditions. We first calculated the difference between the *r*-squares of the experimental conditions and selected all time-frequency points whose absolute values were larger than a set threshold (see below for the selection of the threshold). Then, the selected samples were clustered in connected sets on the basis of temporal and frequency adjacency. The cluster-level statistics were finally calculated by taking the sum of the *r*-squares within each cluster.

The nonparametric statistics were performed by calculating a permutation test where the experimental conditions were randomly intermixed within each subject. The *r*-squares were then calculated for these two permuted conditions, and the difference between the *r*-squares of these two fictional conditions was stored. This procedure was repeated 5,000 times. For each of these permutations, a cluster analysis similar to that described above was performed. Finally, the *P* values were calculated by comparing the values of the cluster-level statistics of our original data with the cluster-level statistics of all permutations. The rationale behind this test is that if no true difference between experimental conditions exists, then similar sized clusters should appear in the permuted data sets. It is important to note that the *P* values for all clusters are calculated under the permutation distribution of the maximum (absolute value) cluster-level statistic. The choice for the maximum cluster-level statistic results in a statistical test that controls the false-alarm rate for all clusters (Maris and Oostenveld 2007). However, this control comes at the expense of a reduced sensitivity for smaller clusters.

As mentioned before, this analysis depends on a chosen threshold for which all values above are considered as possible candidates for the clusters. To set the threshold, we collapsed the absolute values of the differential *r*-squares from all time points and frequencies from all 5,000 permutations and selected the 99. 5th percentile of the distribution. Importantly, this threshold does not affect the false-alarm rate of the statistical test (Maris and Oostenveld 2007), although it does affect the sensitivity of the test.

RESULTS

Behavioral results. Reaction times (RTs) for correct responses from the two probability distributions (Fig. 1*C*) were submitted to a repeated-measures ANOVA with probability distribution (*U*-shaped and negatively skewed) and FP (1.25, 2.25, and 3.25 s) as factors. We found a significant main effect of FP [$F(2,22) = 80.70$; $P < 0.001$], showing the classical effect: decreasing RTs with increasing FP (Niemi and Naatanen 1981). There was also a significant main effect of probability distribution [$F(1,11) = 8.51$; $P < 0.05$] and a significant interaction between the factors [$F(2,22) = 11.66$; $P < 0.001$]. Consistent with the anticipation functions, subsidiary analyses showed a significant difference between the distributions only in the first FP ($P < 0.01$, Bonferroni corrected). Moreover, in both distributions, subjects were significantly slower in the first FP compared with the second and third FP ($P < 0.001$, Bonferroni corrected). However, only in the negatively skewed distribution were subjects significantly slower in the second FP compared with the third ($P < 0.01$, Bonferroni corrected).

CNV. Figure 1*D* summarizes the effects of evolving temporal expectations on the CNV. In line with previous literature, the CNV was more pronounced in central-midline electrodes (Los and Heslenfeld 2005; Miniussi et al. 1999; Trillenberg et al. 2000). In particular, we were interested in whether the CNV would be different at the first FP, where we found a significant difference between RTs. Neural activity associated with the CNV was calculated as the average amplitude between −100 ms to 100 ms around each of the two first possible moments of

target occurrence for the Cz electrode (Fig. 1*D*). We did not analyze the last FP to avoid the potential being contaminated by target-related processing. Based on previous studies, we expected that the different anticipation functions would give rise to different temporal developments of the CNV, with larger amplitudes at moments of high temporal expectations (Trillenberg et al. 2000). Modulation of the CNV was tested using a repeated-measures ANOVA with probability distribution (*U*-shaped, negatively skewed) and FP (1.25, 2.25) as factors. There was a significant main effect of FP [$F(1,11) = 12.55$; $P < 0.01$], indicating that the CNV became larger (more negative) as a function of the FP. We also found a significant main effect of probability distribution [$F(1,11) = 8.45$; $P < 0.05$] and a significant interaction between the factors [$F(1,11) = 5.54$; $P < 0.05$]. Similar to the RT results, subsidiary analyses showed a significant difference between the distributions only in the first FP ($P < 0.001$, Bonferroni corrected). Figure 1*D* shows how the potential was steeper in the *U*-shaped distribution, revealing that it developed gradually and peaked at the anticipated time of the relevant target or response (Los and Heslenfeld 2005; Macar and Vidal 2004; Pfeuty et al. 2005; Trillenberg et al. 2000). The CNV was also significantly more negative in the second FP than in the first FP in both distributions ($P < 0.05$, Bonferroni corrected).

Theta power and PLV. Figure 2 shows the temporal development and scalp distribution of theta power and PLVs across conditions. Time-frequency analysis revealed that theta oscillations were strongest over central-midline electrodes (Cohen et al. 2007; Debener et al. 2005; Luu et al. 2004; Tsujimoto et al. 2006, 2010). Theta amplitude at the Cz electrode was averaged from 4 to 8 Hz, from −100 ms to 100 ms around the two first FPs. The averaged increase of power relative to baseline (from −250 ms to WS onset) was submitted to a repeated-measures ANOVA with probability distribution (*U*-shaped, negatively skewed) and FP (1.25, 2.25) as factors.

There was a significant main effect of probability distribution [$F(1,11) = 5.02$; $P < 0.05$] and FP [$F(1,11) = 14.96$; $P < 0.01$] and an interaction between the two factors [$F(1,11)$ 5.21; $P < 0.05$]. In agreement with RT and CNV results, subsidiary analyses showed a significant difference between the distributions only in the first FP ($P < 0.01$, Bonferroni corrected). Moreover, only the negatively skewed distribution showed a difference between the FPs ($P < 0.01$, Bonferroni corrected). In accordance with the anticipation functions, we found that the difference in theta synchronization between distributions was restricted to the first FP, where the expectation of a target and associated decision and motor response was strongest. We can observe how the theta power increases earlier in the *U*-shaped condition than in the negatively skewed condition. Similarly to the CNV, the theta power ramped up gradually and peaked at the anticipated times of possible presentation of targets. To test the temporal specificity of this effect, we used a cluster-based analysis (Maris and Oostenveld 2007) to compare theta activity (4–8 Hz) between conditions across the time period of 0.75 s and 3 s after WS. We found that theta power was significantly higher in the *U*-shaped condition between 1.1 s and 1.4 s after WS (cluster $P < 0.05$).

To measure how consistent the phases of ongoing oscillations were across different trials, we used the PLV (also called phase-locking factor or intertrial coherence). This index can take values between 0 and 1, where a value of 0 represents

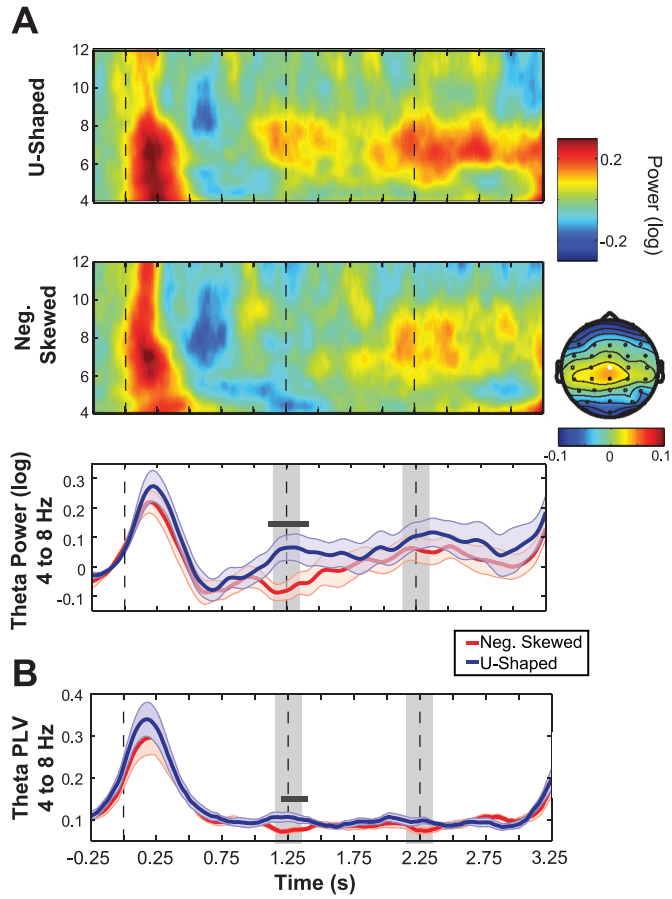

Fig. 2. *A*: time-frequency representation of the theta-band power at electrode Cz. *Bottom*: averaged activity over 4 Hz to 8 Hz. Time window of interest was defined at −100 to 100 ms around the 2 first FPs (grey patches at *bottom*). Thick grey lines represent temporal clusters where there was a significant difference between conditions. There was significant difference between conditions only in the first time window. Scalp distribution shows theta power averaged across both conditions and FPs. *B*: averaged phase-locking values (PLV) activity over 4 to 8 Hz at electrode Cz. PLV is an index of how concentrated the data sample is around the mean direction. Higher values indicate more synchronization across trials. Time window of interest was defined at −100 to 100 ms around the at first FPs (grey patches at *bottom*). Thick grey lines represent temporal clusters where there was a significant difference between conditions.

absence of synchronization across trials, and a value of 1 indicates perfect synchronization. The PLV at the Cz electrode was averaged from 4 to 8 Hz from −100 to 100 ms around the two first FPs (Fig. 2*B*). These values were submitted to a repeated-measures ANOVA with probability distribution (*U*-shaped, negatively skewed) and FP (1.25, 2.25) as factors. There was a main effect of probability distribution [$F(1,11) = 10.34$; $P < 0.01$] and no significant main effect of FP [$F(1,11) = 0.15$; $P > 0.5$]. The interaction between the factors was also not significant [$F(1,11) = 0.72$; $P > 0.5$]. Similar to theta power, we also tested the temporal specificity of this effect by means of a cluster-based analysis (Maris and Oostenveld 2007). We found that theta PLV was significantly higher in the *U*-shaped condition between 1.2 s and 1.4 s after WS (cluster $P < 0.05$).

To test the frequency specificity of these effects, we further compared PLV and power between conditions for delta (1 to 4 Hz), alpha (8 to 12 Hz), and beta (15 to 30 Hz) using a similar cluster-based analysis as used for theta. We found no signifi-

cant difference between conditions for power or PLV (cluster $P > 0.18$).

Phase-power coupling. It is increasingly accepted that the phase-power coupling between low- and high-frequency brain oscillations can be an effective mechanism to coordinate activity in distributed cortical areas (Canolty et al. 2006; Canolty and Knight 2010). Given the significant modulation of theta-band activity related to the differences in temporal expectation, we tested for modulations in phase-power coupling between theta and high-frequency activity in the beta band related to motor excitability.

As previously described, the analysis of phase-power coupling was completed in two steps. In a first step, we investigated whether there was a consistent phase-power coupling between theta phase from electrode Cz and beta-power from electrode C3, placed over motor cortex contralateral to the response hand. Phase and power values were collapsed for the period between 1 and 3 s after WS and across experimental conditions. Figure 3*A* shows how the power within the beta range was nested in theta phase. Specifically, the coupling peaked for theta frequency ~5 Hz.

To investigate how this phase-power coupling developed over time in the different probability distributions, we calculated the circular-linear correlation between the phase of theta (5 Hz) and the power of beta for sequential time windows after the WS. Therefore, we could test: *1*) whether there was a significant phase-power coupling between theta and beta; *2*) whether this coupling increased/decreased in time; and *3*) whether the time course of this coupling differed between probability distributions.

Figure 3*B* shows that the nesting of beta power in theta phase was strongly modulated by the probability distribution. Figure 3*C* shows the difference of the circular-linear correlation coefficients (*r*-squares) between the two conditions. Because the properties of the circular-linear correlation coefficient are very different from the linear correlation coefficient (Busch and VanRullen 2010), we used cluster-based nonparametric test to assess the statistical difference between conditions (Maris and Oostenveld 2007). We found a significantly higher coupling in the *U*-shaped distribution in a first cluster that occurred approximately between 1.4 and 2 s in the beta range ($P < 0.01$). Although coupling appeared higher in the negatively skewed distribution in a second cluster shown in Fig. 3*B*, this observation was not statistically reliable ($P > 0.3$).

Figure 4 shows the distribution of beta power within theta-phase angle for the period between 1.5 and 2 s in the different probability distributions. While there was a marked pattern of power distribution within theta phase angles in the *U*-shaped condition, no such pattern was observed in the negatively skewed condition.

To exclude the possibility of this nesting being due to an increase of phase concentration or power increase of the frequencies involved, we also performed a series of control analyses. The analyses were performed on the PLV and power-amplitude values of theta (5 Hz) at electrode Cz and power of beta (15 to 25 Hz) at electrode C3. For all analyses, the data (power or PLV) were averaged over the periods of 1.5 to 2 s and 2.5 and 3 s after the WS. The values were then submitted to a repeated-measures ANOVA with probability distribution (*U*-shaped, negatively skewed) and interval (1.5 to 2 s and 2.5 to 3 s) as factors. None of these control analyses showed any effects that could have contaminated our phase-power coupling results. The PLV analysis of theta showed no significant main effects {probability distribution [$F(1,11) = 1.225$; $P > 0.29$], interval [$F(1,11) = 0.13$; $P > 0.7$], or interaction [$F(1,11) = 0.54$; $P > 0.4$]} between the factors. Similarly, no significant effects or interaction were found on the analysis of theta power {probability distribution: [$F(1,11) = 0.74$; $P > 0.4$], interval [$F(1,11) = 2.29$; $P > 0.16$], and interaction [$F(1,11) = 0.02$; $P > 0.9$]}. Analysis of the beta power showed a marginal effect of interval [$F(1,11) = 4.23$; $P = 0.064$] but no significant effect of probability distribution [$F(1,11) = 1.20$; $P = 0.296$] or interaction between the factors [$F(1,11) = 2.94$; $P > 0.11$]. The marginal effect of interval suggested that beta power was more desynchronized on the second period (from 2.5 to 3 s after the WS) than on the first period (from 1.5 to 2 s after WS, see Supplemental Information; Supplemental Material for this article is available online at the *J Neurophysiol* website). This result cannot account for the differences found in phase-power coupling, which show that the strongest difference of nesting between conditions occurred in the first period, where theta power, theta PLV, and beta power were not significantly different between conditions.

Given the strong coupling between theta phase and beta power, we further investigated whether there was a relation between temporal expectations and phase-power coupling. If this phase-power coupling serves as mechanism of motor reprogramming and updating, then higher temporal expectation should be followed by higher motor reprogramming. We used the theta power around the first FP (1.15 to 1.35 s after WS) of the *U*-shaped condition as an index of temporal expectation. Because phase-power coupling was distinctly high in the *U*-shaped distribution, we focused our analyses in this condition. After dividing the trials into high and low theta power, we compared the phase-power coupling values between them. The coupling was measured around the time period where there was significant phase-power coupling in the *U*-shaped condition (1.4 to 1.8 s after WS). To assess the statistical difference between the *r*-squares on trials with high and low temporal expectations, we performed a nonparametric cluster analysis, similar to that performed in the phase-power coupling analysis (Maris and Oostenveld 2007). The statistics were performed by comparing the difference between trials with high and low theta power to the differences obtained when trials were randomly intermixed within each subject. We found that phase-power coupling between theta and beta was significantly higher in trials with higher theta power around the first FP ($P < 0.05$). Importantly, this difference was confined to beta power (14.5 to 22 Hz). It could be argued that overall higher theta power would lead to a better estimation of phase in theta, which in turn could lead to a better estimation of the phase-power coupling values in our results. Therefore, as a control, we performed a similar analysis, but now the median split was based on theta power during the high coupling period (1.55 to 1.75 s after WS). We found no significant clusters between coupling of theta and beta on trials with high and low theta power.

DISCUSSION

In the present study, we investigated the neural mechanisms of temporal expectations and their influence over motor prep-

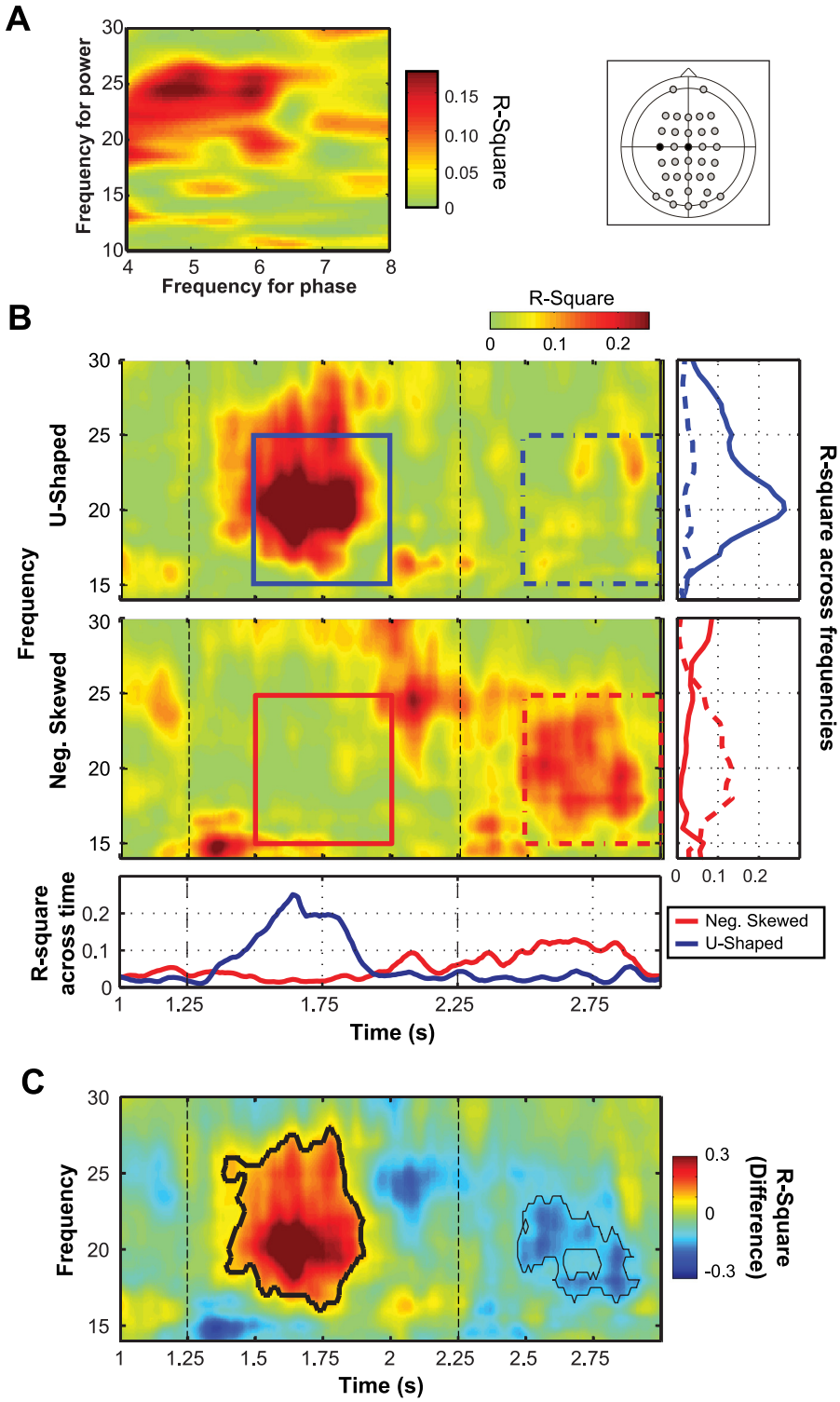

Fig. 3. *A*: phase-power coupling between theta phase and beta power. Representation of the circular-linear coefficient (*r*-square) between theta-phase angle (4–8 Hz) at electrode Cz and higher frequencies power (10 to 30 Hz) at electrode C3. The *r*-squares were calculated for the time period between 1 to 3 s after WS and collapsed over experimental conditions. *B*: representation of the circular-linear coefficient (*r*-square) between theta-phase angle (5 Hz) at electrode Cz and beta power (14 Hz to 30 Hz) at electrode C3. The *r*-squares were calculated for overlapping time windows of 600 ms from 1 to 3 s after WS presentation. *Bottom*: *r*-square across time averaged over 15 to 25 Hz. *Right*: *r*-square across frequencies averaged for the period from 1.5 to 2 s (continuous line) and 2.5 to 3 s (dashed line). *C*: difference of the *r*-square between conditions (*U*-Shaped − Neg. Skewed). Contours indicate the 2 clusters where the *r*-square were different between conditions. First cluster reached significance ($P < 0.01$), while the second was not statistically significant ($P > 0.3$).

aration and updating. The behavioral data confirmed the modulation of RTs by temporal expectations governed by the hazard rates (Bueti et al. 2010; Janssen and Shadlen 2005; Los and Heslenfeld 2005; Luce 1986; Nobre et al. 2007; Trillenberg et al. 2000). Slow brain potentials (CNV) varied according to the anticipation functions, reinforcing their relationship with temporal expectations (Los and Heslenfeld 2005; Miniussi et al. 1999; Pfeuty et al. 2005; Praamstra et al. 2006; Trillenberg et al. 2000; Walter et al. 1964). Our time-frequency analysis showed that low-frequency oscillations also reflected the temporal anticipation functions, suggesting that these oscillations can provide a central mechanism for temporal expectations by encoding the anticipation rate. Moreover, these low-frequency oscillations were coupled with beta power in specific time points, possibly as a mechanism of motor updating (Canolty and Knight 2010).

Slow brain potentials. The CNV is thought to be generated in brain areas related to motor preparation and has been

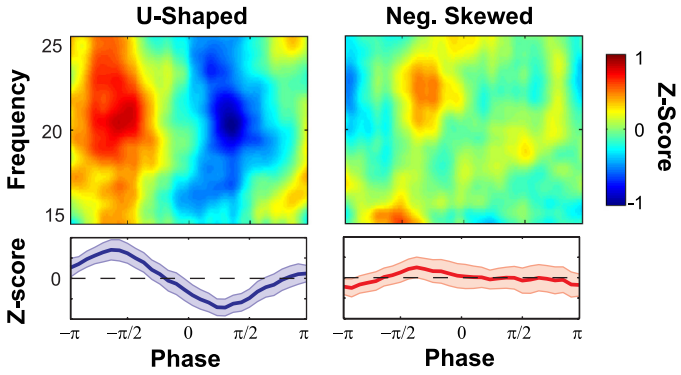

Fig. 4. Distribution of beta power over the phases of theta. Representation of the relationship between theta-phase angle and beta power (15 to 25 Hz) on both experimental conditions over the period from 1.5 to 2 s (continuous squares on Fig. 4). Colormaps shows how the power of beta was distributed over the phase angles of theta. *Bottom*: averaged z-score over beta power (15 to 25 Hz) for theta-phase angle.

traditionally linked to nonspecific preparation (Los and Heslenfeld 2005; Nagai et al. 2004; Nobre 2001; Pfeuty et al. 2005; Praamstra et al. 2006). We found that this potential ramped up gradually after the WS and its amplitude and time course were strongly related to the target presentation schedule. Our observation is in line with several others, suggesting that general preparation was strongly influenced by changes in the ongoing temporal expectation inherent to the task (Los and Heslenfeld 2005; Miniussi et al. 1999; Praamstra et al. 2006; Trillenberg et al. 2000). These findings are well rooted in the literature, giving us confidence in the results from new, further analyses that consider how modulation of oscillatory brain activity may contribute to these well-established findings.

Low-frequency oscillations. While high-frequency oscillations are confined to a small neuronal space due the limited speed of neuronal communication, low-frequency oscillations can modulate activity over large spatial scales over long temporal windows (Buzsaki 2006; Buzsaki and Draguhn 2004; Canolty and Knight 2010). Synchronization of low-frequency oscillations, such as theta, can have profound effects in regulating cortical excitability at a large scale and may serve as a mechanism for temporal preparation (Buzsaki and Draguhn 2004; Canolty and Knight 2010; Schroeder and Lakatos 2009). In support of this idea, here we found an increase in theta power as a function of the anticipation rate. Interestingly, theta power was highest in anticipation of critical moments where the target could be presented.

We also found a significant increase in the PLV of theta oscillations in periods where there was a marked difference in the temporal expectations between conditions. High phase concentration around a mean angle is commonly associated with phase reset caused by a stimulus (Tallon-Baudry and Bertrand 1999). In our design, however, no stimulus appeared during the time period analyzed. The results therefore suggest that resetting of the theta phase occurred as a consequence of an endogenous signal related to the expected occurrence of a target. Moreover, it was possible to determine that the main reason for the difference between PLVs around the first FP between conditions was a relative increase of this index in the *U*-shaped distribution.

The higher increase took place in a time period similar to the significant differences of the CNV. Our findings support the hypothesis that the slow CNV potential may reflect the underlying low-frequency carrier oscillations (Praamstra et al. 2006; Schroeder and Lakatos 2009). The CNV (as other ERPs) is probably not the effect of a single oscillation but rather the sum of various localized cortical EEG processes. Nevertheless, a reproducible potential in the averaged ERP should be partly due to phase locking of the contributing process activities to the time-locking events in one or more frequency regions (Makeig et al. 2004).

Theta distributed over the frontal-midline scalp has been implicated in a number of functions, such as memory load (Jensen and Tesche 2002), attentional demand (Sauseng et al. 2007; Tsujimoto et al. 2010), error monitoring (Debener et al. 2005; Luu et al. 2004), reward expectation (Cohen et al. 2007; Hollerman and Schultz 1998; Tsujimoto et al. 2006), and motor readiness (Yamanaka and Yamamoto 2010a,b). Although some argue that formulating a theory that can attribute a specific cognitive function to frontal-midline theta is difficult (Mitchell et al. 2008), we can observe that many of these cognitive functions have in common coordinating excitability across multiple areas and specifically coordinating excitability in time. For example, in error monitoring and reward expectations, there is an intrinsic temporal structure involved. Therefore, we suggest that theta power can play a key role in temporally coordinating excitation, which in turn can be used for different task relevant purposes.

Phase-power coupling. Low frequency oscillations can modulate activity over large spatial regions in long temporal windows while high-frequency oscillations can modulate activity over small spatial regions and short temporal windows (Canolty and Knight 2010). Therefore, it has been suggested that the coupling of these features can serve as a mechanism to transfer information from large-scale brain networks to the fast, local cortical processing required for effective computation (Buzsaki and Draguhn 2004; Canolty and Knight 2010) .

The marked coupling between theta and beta found in this study seems to fit well this view. As previously discussed, theta oscillations may reflect a general state of increasing expectation. Beta oscillations, on the other hand, have been consistently related to motor preparation and inhibition (Pfurtscheller et al. 1996; Sanes and Donoghue 1993; Swann et al. 2009; Tzagarakis et al. 2010; Wang 2010) and, in a more general view, to the maintenance of the current sensorimotor or cognitive state (Engel and Fries 2010). Given that an increase in the coupling between these frequencies occurred after moments of high temporal expectation, we speculate that it might be related to motor reprogramming when the temporal expectations encoded in the lower oscillations are not fulfilled. Importantly, we found that higher theta power, linked to greater temporal expectation, was followed by higher theta-beta coupling, suggesting that the nesting of power within the phase of slow oscillatory activity can serve for motor updating: stronger reprogramming happened when participants had higher temporal expectations. This mechanism might serve as a general endogenous prediction error for events expected over time. In fact, studies have shown that reward-related prediction errors track not only the occurrence or absence of a reward but also its expected time (Hollerman and Schultz 1998).

Moreover, although it has been repeatedly suggested that the coupling between frequencies should be transient due to the scale-free dynamics of brain activity (Canolty and Knight 2010; He et al. 2010; Kayser and Ermentrout 2010), not many studies have actually measured this coupling over time. Be-

cause we analyzed solely trials where the target was presented on the last FP, we were able to observe the temporal development of this coupling without any contamination of evoked activity. In addition of the finding that the coupling is in fact transient, we also found that increases in coupling happened in very specific task-relevant time points. This shows a temporally specific, dynamic mechanism at work.

In conclusion, we support the notion that nesting of high-frequency activity within low-frequency oscillations can provide a general mechanism for controlling cortical excitability (Canolty and Knight 2010; Schroeder and Lakatos 2009). Furthermore, we suggest this mechanism allows the timing of neural excitability to precise temporal moments, according to environmental regularities and in a dynamic and adaptive way.

GRANTS

This work was supported by Wellcome Trust project grant (to A. C. Nobre). G. Rohenkohl was partially supported by Programme Alban (the European Union Programme of High Level Scholarship for Latin America No. E07D403637BR). A. M. Cravo was supported by Fundação de Amparo à Pesquisa do Estado de São Paulo (FAPESP) and CAPES. V. Wyart was supported by the Fyssen Foundation.

DISCLOSURES

No conflicts of interest, financial or otherwise, are declared by the author(s).

REFERENCES

AEEGS. American Electroencephalographic Society guidelines for standard electrode position nomenclature. *J Clin Neurophysiol* 8: 200–202, 1991.

Alegre M, Imirizaldu L, Valencia M, Iriarte J, Arcocha J, Artieda J. Alpha and beta changes in cortical oscillatory activity in a go/no go randomly-delayed-response choice reaction time paradigm. *Clin Neurophysiol* 117: 16–25, 2006.

Berens P. CircStat: A MATLAB toolbox for circular statistics. *J Stat Software* 31: 1–21, 2009.

Bueti D, Bahrami B, Walsh V, Rees G. Encoding of temporal probabilities in the human brain. *J Neurosci* 30: 4343–4352, 2010.

Busch NA, VanRullen R. Spontaneous EEG oscillations reveal periodic sampling of visual attention. *Proc Natl Acad Sci USA* 107: 16048–16053, 2010.

Buzsaki G. *Rhythms of the Brain*. Oxford, UK: Oxford University Press, 2006.

Buzsaki G, Draguhn A. Neuronal oscillations in cortical networks. *Science* 304: 1926–1929, 2004.

Canolty RT, Edwards E, Dalal SS, Soltani M, Nagarajan SS, Kirsch HE, Berger MS, Barbaro NM, Knight RT. High gamma power is phase-locked to theta oscillations in human neocortex. *Science* 313: 1626–1628, 2006.

Canolty RT, Knight RT. The functional role of cross-frequency coupling. *Trends Cogn Sci* 14: 506–515, 2010.

Cohen M, Elger C, Ranganath C. Reward expectation modulates feedback-related negativity and EEG spectra. *Neuroimage* 35: 968–978, 2007.

Cotti J, Rohenkohl G, Stokes M, Nobre AC, Coull JT. Functionally dissociating temporal and motor components of response preparation in left intraparietal sulcus. *Neuroimage* 54: 1221–1230, 2011.

Cui X, Stetson C, Montague PR, Eagleman Ready DM. Go: amplitude of the fMRI signal encodes expectation of cue arrival time. *PLoS Biol* 7: e1000167, 2009.

Debener S, Ullsperger M, Siegel M, Fiehler K, Cramon DYv, Engel AK. Trial-by-trial coupling of concurrent electroencephalogram and functional magnetic resonance imaging identifies the dynamics of performance monitoring. *J Neurosci* 25: 11730–11737, 2005.

Engel AK, Fries P. Beta-band oscillations–signalling the status quo? *Curr Opin Neurobiol* 20: 156–165, 2010.

Gibbon J. Scalar expectancy theory and Weber's law in animal timing. *Psychol Rev* 84: 279–325, 1977.

He BJ, Zempel JM, Snyder AZ, Raichle ME. The temporal structures and functional significance of scale-free brain activity. *Neuron* 66: 353–369, 2010.

Hollerman JR, Schultz W. Dopamine neurons report an error in the temporal prediction of reward during learning. *Nature* 1: 304–308, 1998.

Janssen P, Shadlen MN. A representation of the hazard rate of elapsed time in macaque area LIP. *Nat Neurosci* 8: 234–241, 2005.

Jensen O, Tesche C. Frontal theta activity in humans increases with memory load in a working memory task. *Eur J Neurosci* 15: 1395–1399, 2002.

Kayser C, Ermentrout B. Complex times for earthquakes, stocks, and the brain's activity. *Neuron* 66: 329–331, 2010.

Killeen PR, Weiss NA. Optimal timing and the Weber function. *Psychol Rev* 94: 455–468, 1987.

Lakatos P, Chen CM, O'Connell MN, Mills A, Schroeder CE. Neuronal oscillations and multisensory interaction in primary auditory cortex. *Neuron* 53: 297–292, 2007.

Lakatos P, Karmos G, Mehta AD, Ulbert I, Schroeder CE. Entrainment of neuronal oscillations as a mechanism of attentional selection. *Science* 320: 110–113, 2008.

Lakatos P, Shah AS, Knuth KH, Ulbert I, Karmos G, Schroeder CE. An oscillatory hierarchy controlling neuronal excitability and stimulus processing in the auditory cortex. *J Neurophysiol* 94: 1904–1911, 2005.

Los SA, Heslenfeld DJ. Intentional and unintentional contributions to nonspecific preparation: Electrophysiological evidence. *J Exp Psychol* 134: 52–72, 2005.

Luce RD. *Response Times: Their Role in Inferring Elementary Mental Organization*. New York: Oxford University Press, 1986.

Luu P, Tucker DM, Makeig S. Frontal midline theta and the error-related negativity: neurophysiological mechanisms of action regulation. *Clin Neurophysiol* 115: 1821–1835, 2004.

Macar F, Vidal F. Event-related potentials as indices of time processing: a review. *J Psychophysiol* 18: 89–104, 2004.

Makeig S, Delorme A, Westerfield M, Jung TP, Townsend J, Courchesne E, Sejnowski TJ. Electroencephalographic brain dynamics following manually responded visual targets. *PLoS Biol* 2: e176, 2004.

Maris E, Oostenveld R. Nonparametric statistical testing of EEG- and MEG-data. *J Neurosci Methods* 164: 177–190, 2007.

Miniussi C, Wilding EL, Coull JT, Nobre AC. Orienting attention in time–modulation of brain potentials. *Brain* 122: 1507–1518, 1999.

Mitchell DJ, McNaughton N, Flanagan D, Kirk IJ. Frontal-midline theta from the perspective of hippocampal ''theta''. *Prog Neurobiol* 86: 156–185, 2008.

Nagai Y, Critchley HD, Featherstone E, Fenwick PB, Trimble MR, Dolan RJ. Brain activity relating to the contingent negative variation: an fmri investigation. *Neuroimage* 21: 1232–1241, 2004.

Niemi P, Naatanen R. Foreperiod and simple reaction-time. *Psychol Bull* 89: 133–162, 1981.

Nobre AC. Orienting attention to instants in time. *Neuropsychologia* 39: 1317–1328, 2001.

Nobre AC, Correa A, Coull JT. The hazards of time. *Curr Opin Neurobiol* 17: 465–470, 2007.

Pfeuty M, Ragot R, Pouthas V. Relationship between CNV and timing of an upcoming event. *Neurosci Lett* 382: 106–111, 2005.

Pfurtscheller G, Stancák A, Neuper C. Post-movement beta synchronization. A correlate of an idling motor area? *Electroencephalogr Clin Neurophysiol* 98: 281–293, 1996.

Poli S, Sarloa M, Bortolettoa M, Buodoa G, Palombaa D. Stimulus-preceding negativity and heart rate changes in anticipation of affective pictures. *Int J Psychophysiol* 65: 32–39, 2007.

Praamstra P, Kourtis D, Kwok HF, Oostenveld R. Neurophysiology of implicit timing in serial choice reaction-time performance. *J Neurosci* 26: 5448–5455, 2006.

Riehle A, Grun S, Diesmann M, Aertsen A. Spike synchronization and rate modulation differentially involved in motor cortical function. *Science* 278: 1950–1953, 1997.

Sanes J, Donoghue J. Oscillations in local field potentials of the primate motor cortex during voluntary movement. *Proc Natl Acad Sci USA* 90: 4470–4474, 1993.

Sauseng P, Hoppe J, Klimesch W, Gerloff C, Hummel FC. Dissociation of sustained attention from central executive functions: local activity and interregional connectivity in the theta range. *Eur J Neurosci* 25: 587–593, 2007.

Schroeder CE, Lakatos P. Low-frequency neuronal oscillations as instruments of sensory selection. *Trends Neurosci* 32: 9–18, 2009.

Swann N, Tandon N, Canolty R, Ellmore T, McEvoy L, Dreyer S, DiSano M, Aron A. Intracranial EEG reveals a time and frequency specific role for

the right inferior frontal gyrus and primary motor cortex in stopping initiated responses. *J Neurosci* 29: 12675–12685, 2009.

Tallon-Baudry C, Bertrand O. Oscillatory gamma activity in humans and its role in object representation. *Trends Cogn Sci* 3: 151–162, 1999.

Trillenberg P, Verleger R, Wascher E, Wauschkuhn B, Wessel K. CNV and temporal uncertainty with "ageing" and "non-ageing" S1–S2 intervals. *Clin Neurophysiol* 111: 1216–1226, 2000.

Tsujimoto T, Shimazu H, Isomura Y. Direct recording of theta oscillations in primate prefrontal and anterior cingulate cortices. *J Neurophysiol* 95: 2987–3000, 2006.

Tsujimoto T, Shimazu H, Isomura Y, Sasaki K. Theta oscillations in primate prefrontal and anterior cingulate cortices in forewarned reaction time tasks. *J Neurophysiol* 103: 827–843, 2010.

Tzagarakis C, Ince NF, Leuthold AC, Pellizzer G. Beta-band activity during motor planning reflects response uncertainty. *J Neurosci* 30: 11270–11277, 2010.

van Ede F, de Lange F, Jensen O, Maris E. Orienting attention to an upcoming tactile event involves a spatially and temporally specific modulation of sensorimotor alpha- and beta-band oscillations. *J Neurosci* 31: 2016–2024, 2011.

Walter W, Cooper R, Aldridge V, McCallum W, Winter A. Contingent negative variation: an electrical sign of sensorimotor association and expectancy in the human brain. *Nature* 203: 380–384, 1964.v

Wang XJ. Neurophysiological and Computational Principles of Cortical Rhythms in Cognition. *Physiol Rev* 90: 1195–1268, 2010.

Yamanaka K, Yamamoto Y. Lateralised EEG power and phase dynamics related to motor response execution. *Clin Neurophysiol* 121: 1711–1718, 2010a.

Yamanaka K, Yamamoto Y. Single-trial EEG power and phase dynamics associated with voluntary response inhibition. *J Cogn Neurosci* 22: 714–727, 2010b.